coatings

MDPI

Article

Cavitation Erosion Resistance of TiSiN/NiTiAlCoCrN Nanomultilayer Films with Different Modulation Periods

Hongjuan Yan *, Lina Si *, Zhaoliang Dou, Ye Yang, Hong Li and Fengbin Liu

School of Mechanical and Materials Engineering, North China University of Technology, Beijing 100144, China; yangye@ncut.edu.cn (Y.Y.)

* Correspondence: yanhj@ncut.edu.cn (H.Y.); silina@ncut.edu.cn (L.S.)

Abstract: In order to explore the effect of modulation period on the structure and properties of TiSiN/NiTiAlCoCrN nanomultilayer films, the films were deposited on 304 stainless steel via a magnetron sputtering system. The structure and element distribution of the films were observed via X-ray diffraction (XRD), scanning electron microscopy (SEM), and energy-dispersive spectroscopy (EDS). The cavitation erosion of the films was investigated using an ultrasonic vibration cavitation machine. The results show that the TiSiN/NiTiAlCoCrN nanomultilayer film exhibits a face-centered cubic (FCC) structure and preferred orientation on the (200) crystal plane. TiSiN/NiTiAlCoCrN nanomultilayer films grow in the form of columnar crystals, which grow perpendicularly to the direction of the substrate. With increasing modulation periods, the hardness, elastic modulus, and adhesive force firstly increase and then decrease. When the modulation period is 11 nm, the TiSiN/NiTiAlCoCrN nanomultilayer film has the biggest hardness of (14.649 ± 0.591) GPa, elastic modulus of (249.065 ± 10.485) GPa, and adhesive force of 11.3 N. With increasing modulation periods, the mass loss firstly decreases and then increases. When the modulation period is 11 nm, the mass loss is the minimum of 0.6 mg. There are two reasons for improving the cavitation erosion resistance of the films. The TiSiN/NiTiAlCoCrN nanomultilayer film has the highest hardness, and the interfaces of the nanomultilayer film can hinder the generation and expansion of cavitation pits.

Keywords: nanomultilayer film; cavitation erosion resistance; modulation period; magnetron sputtering

Citation: Yan, H.; Si, L.; Dou, Z.; Yang, Y.; Li, H.; Liu, F. Cavitation Erosion Resistance of TiSiN/NiTiAlCoCrN Nanomultilayer Films with Different Modulation Periods. *Coatings* **2023**, *13*, 1431. https://doi.org/10.3390/coatings13081431

Academic Editor: Manuel António Peralta Evaristo

Received: 18 July 2023
Revised: 8 August 2023
Accepted: 10 August 2023
Published: 15 August 2023

1. Introduction

Cavitation erosion is commonly found in fluid machine such as turbines and water pumps, and is one of the main reasons of part failure [1,2]. Cavitation erosion induces plastic deformation and micro-cracking in the surface of parts, which shorten the service life of parts [3]. Coatings is one of the effective methods to improve the cavitation erosion resistance of part surfaces [4–7].

The high-entropy alloy (HEA) has become a research focus because of its excellent mechanical properties [8,9], corrosion erosion resistance [10,11], wear resistance [12–14], high temperature oxidation resistance [14,15], and so on. Scratch resistance and wear resistance of AlCoCrFeNi is better than the ones of the substrate [16]. The mass loss of martensite stainless steel is 3.5 times that of the one of AlCoCrFeNi coatings in 3.5 wt% NaCl solution, because the hardness of AlCoCrFeNi coatings is 2 times that of the hardness of martensite stainless steel [17]. CoCrFeNiTiMo coatings have a higher hardness, better adhesive strength, and better cavitation erosion resistance in 3.5 wt% NaCl solution than Ti alloy [18]. Non-metallic elements such as H, N, C, and B are doped into HEA to form HEA composite films, which have better properties due to grain boundary wetting and second-phase strengthening [19–23]. The AlCrTiZrV coating exhibits an amorphous state, but the (AlCrTiZrV)N coating is crystallized and exhibits preferred orientation on the (200) plane. The hardness and elastic modulus of the (AlCrTiZrV)N coating is higher than the ones of the AlCrTiZrV coating [24,25]. Therefore the high-entropy alloy nitride has

excellent properties and can be a modulation layer of nanomultilayer films. The nanomultilayer film can combine the advantages of two materials and has superhardness and excellent properties [26,27]. CrN/CrCN multilayers have a better cavitation erosion than the CrN monolayer [28]. The cavitation erosion resistance of CrAlYN/CrN multilayer coatings improves by a factor of 14 times that of the Ti6Al4V substrate. The main mechanism of cavitation erosion is peel. The interface between multilayer effectively resists shock waves and delays the initiation and propagation of cavitation cracks [5]. Because of the template effect and coherent growth, the (AlCrTiZrV)N/SiC nanomultilayer film has the better mechanical properties [29], and (TiZrNbHfTa)N/WN multilayered nitride coatings have a higher hardness and Young's modulus [30]. The VAlTiCrCu/WC multilayer coating with a modulation period of 17 nm has better adhesion and wear resistance [31]. [AlTiCrNiTa/(AlTiCrNiTa)N]$_{20}$ high-entropy alloy multilayer coatings have a higher hardness and better high temperature oxidation corrosion [32]. The researchers studied the mechanical properties and oxidation corrosion of HEA nitride multilayer film [30–32], but the cavitation erosion of HEA nitrides multilayer films is less reported. Cavitation erosion is one of main reasons for fluid machines. Therefore, the development of the novel film with better cavitation erosion resistance is essential for fluid machines.

The cavitation erosion resistance of NiTiAlCrN film with various nitrogen argon flow ratios was studied. When nitrogen argon flow ratio is 1:1, the dense structure and grain refinement of the NiTiAlCrN film strengthens the hardness and cavitation erosion resistance of the film [33]. On that basis, the TiSiN/NiTiAlCoCrN nanomultilayer film was deposited on the 304 stainless steel substrate. The microstructure, mechanical properties, and cavitation erosion resistance of the films with different modulation periods were studied.

2. Experimental Procedures

2.1. Materials

TiSiN/NiTiAlCoCrN nanomultilayer films with different modulation period were deposited on 304 stainless steel using the JCP-350M2 magnetron sputtering system (Beijing Technol Science Co., Ltd., Beijing, China). The dimension of 304 stainless steel is Φ20 mm × 3 mm and mirror polished. The substrates were cleaned sequentially in distilled water, anhydrous ethanol, and acetone, and they were dried using a blowing machine. The substrates were fixed on the substrate holder. Si content in TiSi target is 10 at.%, and the element content in NiTiAlCoCr target is an equimolar ratio.

2.2. Film Deposition

The vacuum chamber pressure reached 3 × 10^{-3} Pa, and the substrate bias power was adjusted to −600 V. The substrates were etched by Ar^+ for 15 min to remove the impurity and oxidation of substrate surface. The targets were pre-sputtered for 10 min to remove the oxidation of targets. The nitrogen argon flow ratio was 1:1. The TiN layer was deposited on substrate to improve the adhesion between substrate and film. The TiSi target and NiTiAlCoCr target were, respectively, controlled with RF power and DC power. The thickness of TiSiN layer is 3 nm. The modulation periods of NiTiAlCoCrN layer are 5 nm, 7 nm, 9 nm, 11 nm, and 13 nm. The top layer is NiTiAlCoCrN layer, which is deposited for 30 min. The total thickness is about 2 μm. Figure 1 shows the schematic diagram of nanomultilayer film.

2.3. Film Characterization

The structure of the film was observed via Rigaku Ultima IV X-ray diffraction (Tokyo, Japan) with Cu-Kα, 0.15406 nm of wavelength, 40 kV of voltage, 40 mA of current, 8°/mm of sweep velocity, and 20°~100° of sweep angle. Surface and cross-section morphologies were observed via Cart Zeiss Sigma-300 (Oberkochen, Germany) scanning electron microscopy (SEM), and the distribution of elements of deposited film and wear tracks was observed via energy-dispersive spectroscopy (EDS). The hardness and elastic modulus were tested

using an Anton Paar nanoindenter (Graz, Austria) with Berkovich indentor (Graz, Austria), 100 nm of curvature radius, 4 mN of maximum load, and 20 mN/min of loading and unloading speed. In order to eliminate errors, average hardness values were calculated from 5 random points. Adhesive strength was tested using a WS-2005 scratch tester (Zhongke Kaihua Technology Co., Ltd., Lanzhou, China) with 30 N of load, 30 N/min of loading speed, and 3 mm of scratch length. The cavitation erosion experiment was carried out using an ultrasonic vibration cavitation machine with 1200 W of power, 20 Hz of frequency, and 25 μm of amplitude, which is shown in Figure 2. The fluid medium was NaCl 3.5 wt% solution, the distance between film and ultrasonic vibrating head was 0.5 mm, and vibration head diameter was Φ20 mm. The depth of immersion of the sample surface into the fluid medium was about 25 mm. The ice bags were placed around the beaker to maintain the temperature at 25 °C. The mass was tested using a HUAZHI electronic balance (Fuzhou, China) every 2 h of cavitation erosion time. The total time of cavitation erosion time was 12 h.

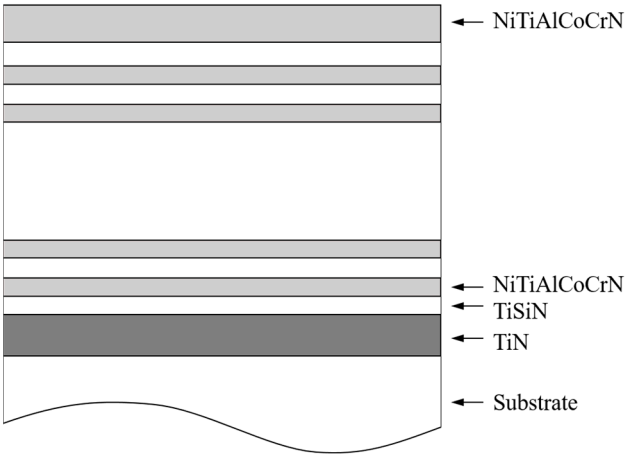

Figure 1. Schematic diagram of nanomultilayer film.

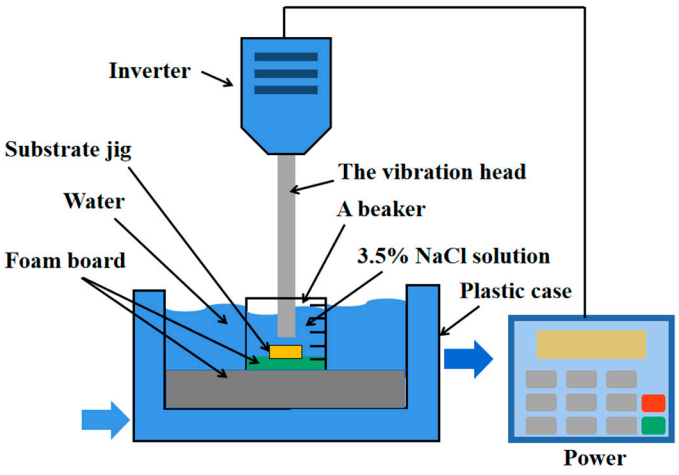

Figure 2. Schematic diagram of ultrasonic vibration machine.

3. Results and Discuss

3.1. Microstructure

Table 1 shows the element distribution of TiSiN/NiTiAlCoCrN nanomultilayer films with different modulation periods. The N element content is from 40.52 at.% to 45.6 at.% in the films. The contents of all metal elements are approximately evenly distributed and consistent with the elemental contents in the targets.

Table 1. Element contents of TiSiN/NiTiAlCoCrN nanomultilayer films.

Modulation Period/nm	Ni /at.%	Error /at.%	Ti /at.%	Error /at.%	Al /at.%	Error /at.%	Cr /at.%	Error /at.%	Co /at.%	Error /at.%	N /at.%	Error /at.%
5 mm	10.60	0.03	10.78	0.02	11.1	0.03	11.38	0.04	10.54	0.03	45.60	0.02
7 mm	10.88	0.06	14.53	0.05	10.77	0.06	12.10	0.02	10.54	0.06	41.18	0.03
9 mm	11.39	0.05	12.31	0.03	11.31	0.05	12.58	0.05	11.11	0.04	41.30	0.06
11 mm	11.59	0.07	12.02	0.03	11.65	0.04	12.47	0.08	11.35	0.02	40.92	0.04
13 mm	11.66	0.04	12.18	0.08	11.52	0.07	12.76	0.03	11.36	0.05	40.52	0.03

Figure 3 shows XRD patterns of TiSiN/NiTiAlCoCrN nanomultilayer films. The films exhibit a face-centered cubic (FCC) structure. The NiTiAlCoCrN film shows preferred orientation on the (111) and (200) planes. The peak of (111) plane of nanomultilayer films disappears, and the nanomultilayer films show preferred orientation on the (200) plane. The nanomultilayer films are mainly composed of Ni_3AlN, $Co_{5.47}N$, TiN, VN, AlN, and CrN phases. The diffraction angle of the (200) plane is from 43.360° to 43.457°, which is close to TiAlN/CrN coatings [34], AlCrN/TiSiN nanomultilayer coatings [26], and AlTiCrN/TiSiN hard coatings [27]. The coherent epitaxial growth appears easily at small modulation periods because of the small mismatch between lattice parameters of NiTiAlCoCrN layer and TiSiN layer [34].

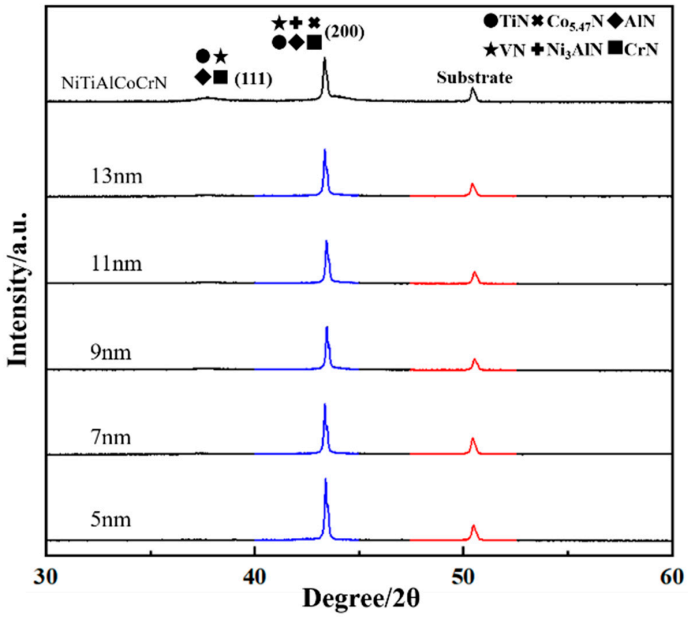

Figure 3. XRD patterns of TiSiN/NiTiAlCoCrN nanomultilayer films (Blue lines show the peak of (200) plane and red lines show the peak of substrate.).

Table 2 shows the diffraction angle, plane spacing, and half-width height of the (200) plane of TiSiN/NiTiAlCoCrN nanomultilayer films. The diffraction angle of the (200) plane first increases and then decreases. The reason is that the TiSiN layer and NiTiAlCoCrN layer grow epitaxially during the deposition process and form a coherent structure on the (200) plane when the modulation period is lower than 11 nm. Lattice distortion appears because of the inconsistent lattice constants of two layer materials. The lattice constant of TiSiN layers increases, and the lattice constant of NiTiAlCoCrN layers decreases. Therefore the tensile compressive alternating stress field is formed during alternating deposition process, which strengthens the properties of the films. With the thickness of the NiTiAlCoCrN layer further increasing, dislocations cannot penetrate the NiTiAlCoCrN layer, and the TiSiN layer and NiTiAlCoCrN layer grow alternatively in a "brick wall" structure during deposition process, which results in properties degradation of the films.

Figure 4 shows the cross-sectional morphologies of the TiSiN/NiTiAlCoCrN nanomultilayer film with different modulation periods. The cross-sectional morphology shows the orderly TiSiN/NiTiAlCoCrN nanomultilayer film, TiN transition layer, and 304 stainless steel substrate from top to bottom. TiSiN/NiTiAlCoCrN nanomultilayer films grow in the form of columnar crystals, which grow perpendicularly to the direction of substrate. When the modulation period is 11 nm, the cross-sectional morphologies exhibit a fine and dense columnar grain structure. However, the cross-sectional morphologies with the other modulation periods show a coarse columnar grain. Therefore, the nanomultilayer film with 11 nm modulation period has the best cross-section.

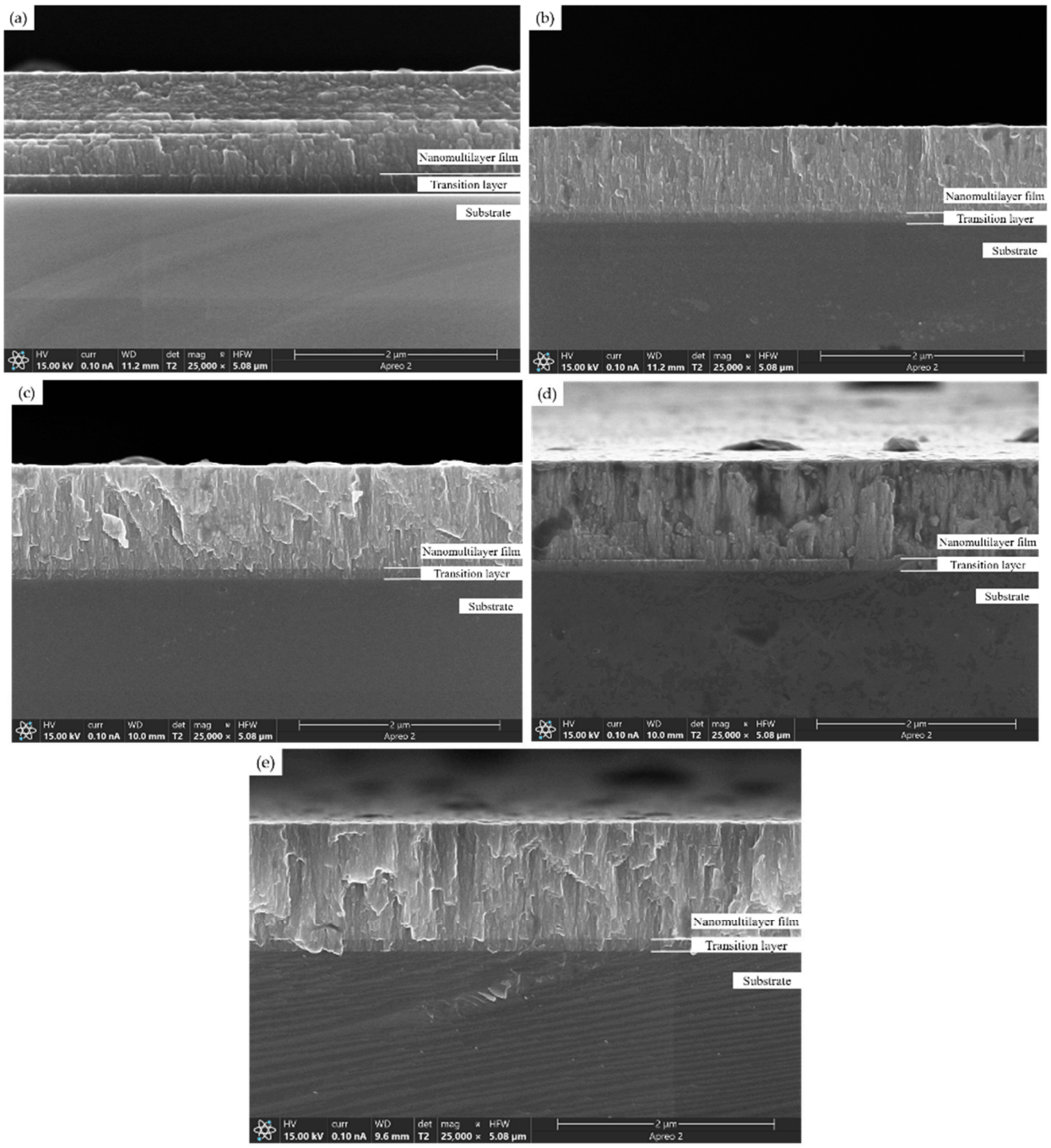

Figure 4. Cross-sectional morphologies of TiSiN/NiTiAlCoCrN nanomultilayer films with different modulation periods: (**a**) 5 nm; (**b**) 7 nm; (**c**) 9 nm; (**d**)11 nm; (**e**) 13 nm.

Table 2. Diffraction angle, plane spacing, and half-width height of (200) plane.

Modulation Period/nm	Diffraction Angle 2θ/(°)	Plane Spacing d/nm	Half-Width Height B/rad
5 nm	43.360	2.0851	0.173
7 nm	43.400	2.0833	0.184
9 nm	43.457	2.0807	0.186
11 nm	43.381	2.0841	0.153
13 nm	43.360	2.0851	0.176

3.2. Mechanical Properties

Figure 5 shows the hardness and elastic modulus. With increasing modulation periods, the hardness and elastic modulus firstly increases and then decreases. When the modulation period is 11 nm, the nanomultilayer film has the highest hardness of (14.649 ± 0.591) GPa and the highest elastic modulus of (249.065 ± 10.485) GPa.

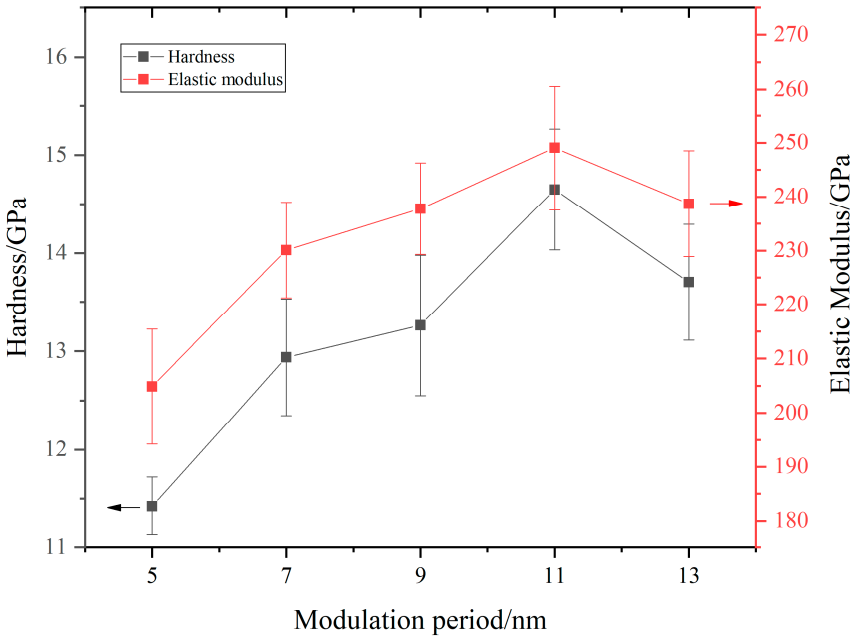

Figure 5. Hardness and elastic modulus of TiSiN/NiTiAlCoCrN nanomultilayer films with different modulation periods.

The strengthening mechanisms of nanomultilayer films include alternating stress field theory [35–37], modulus difference theory [38,39], Hall–Petch theory [40], etc. According to these theories and the results of the microstructure analysis, the plane spacing of TiSiN/NiTiAlCoCrN nanomultilayer films first decreases and then increases. When the plane spacing is lower than 11 nm, the TiSiN layer and NiTiAlCoCrN grow coherently. The TiSiN layer is subjected to compressive stress, while the NiTiAlCoCrN layer is subjected to tensile stress. Therefore, the alternating stress field is formed during the alternating deposition process of two materials, which strengthens the properties of nanomultilayer film. At the same time, the interface between the layers hinders the expansion of dislocations due to the mirror effect of the interlayer interface, which limits the generation and expansion of dislocation and strengthens the properties of the films. With the modulation period further increasing, the template effect disappears. The dislocations move within a monolayer film and accumulate easily in the lower elastic modulus layer. Therefore, the properties of the films decline [38,41].

Figure 6 shows the adhesive force between the nanomultilayer film and substrate. When the modulation period is 11 nm, the adhesive force is at the highest value of 11.3 N.

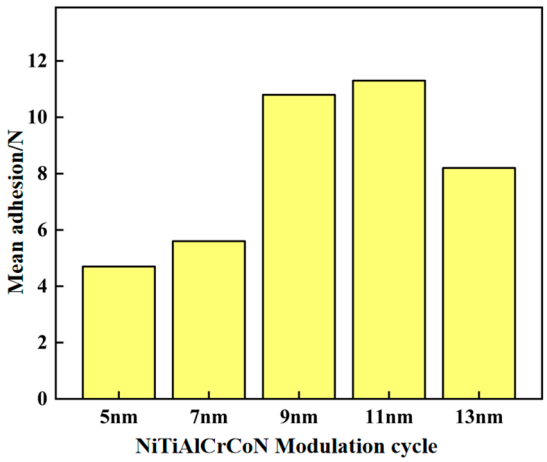

Figure 6. Adhesion force of TiSiN/NiTiAColCrN nanomultilayer film with different modulation periods.

3.3. Corrosion Erosion Resistance

Figure 7 shows relationship between mass loss and time of the TiSiN/NiTiAlCoCrN nanomultilayer film. With increasing modulation period, the mass loss of the films firstly decreases and then increases. When the modulation period of nanomultilayer film is 11 nm, the mass loss is the smallest of 0.6 mg, and the cavitation erosion rate is the smallest of 0.05 mg/h. The nanomultilayer film with 5 nm show the biggest mass loss after 4 h of cavitation erosion. The nanomultilayer film with 7 nm show the biggest mass loss after 12 h of cavitation erosion.

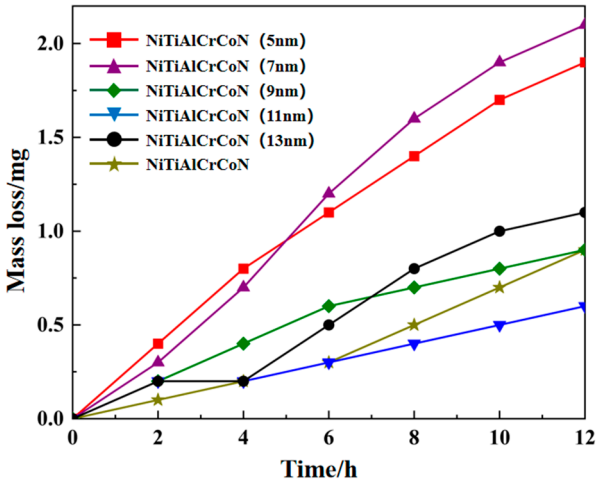

Figure 7. Mass loss of TiSiN/NiTiAlCoCrN nanomultilayer films with different modulation periods.

There are two reasons for the strengthening of the cavitation erosion resistance of the nanomultilayer. Firstly, the nanomultilayer film with an 11 nm modulation period has the highest hardness and adhesive force. Secondly, the films are deposited periodically and alternately by two layers, and therefore, there are many interfaces in the nanomultilayer film. The interfaces prevent the initiation and expansion of cavitation pits, which also improve the cavitation erosion resistance. However, the nanomultilayer film with 5 nm and 7 nm has a lower hardness and elastic modulus, so the mass losses of the nanomultilayer film are bigger than those of the other modulation periods.

Figure 8 shows the surface morphologies of TiSiN/NiTiAlCoCrN nanomultilayer films after 12 h of cavitation erosion. As the modulation period increases, the number of cavitation pits firstly decrease and then increase. When the modulation periods are 5 nm

and 7 nm, there are many cavitation pits, and the expansion of the cavitation pits causes film detachment. When the modulation period is 11 nm, the number of cavitation pits of the TiSiN/NiTiAlCoCrN nanomultilayer film is the least, and the film has not peeled off. So, the film has the best cavitation erosion resistance, which is consistent with the results in Figure 7.

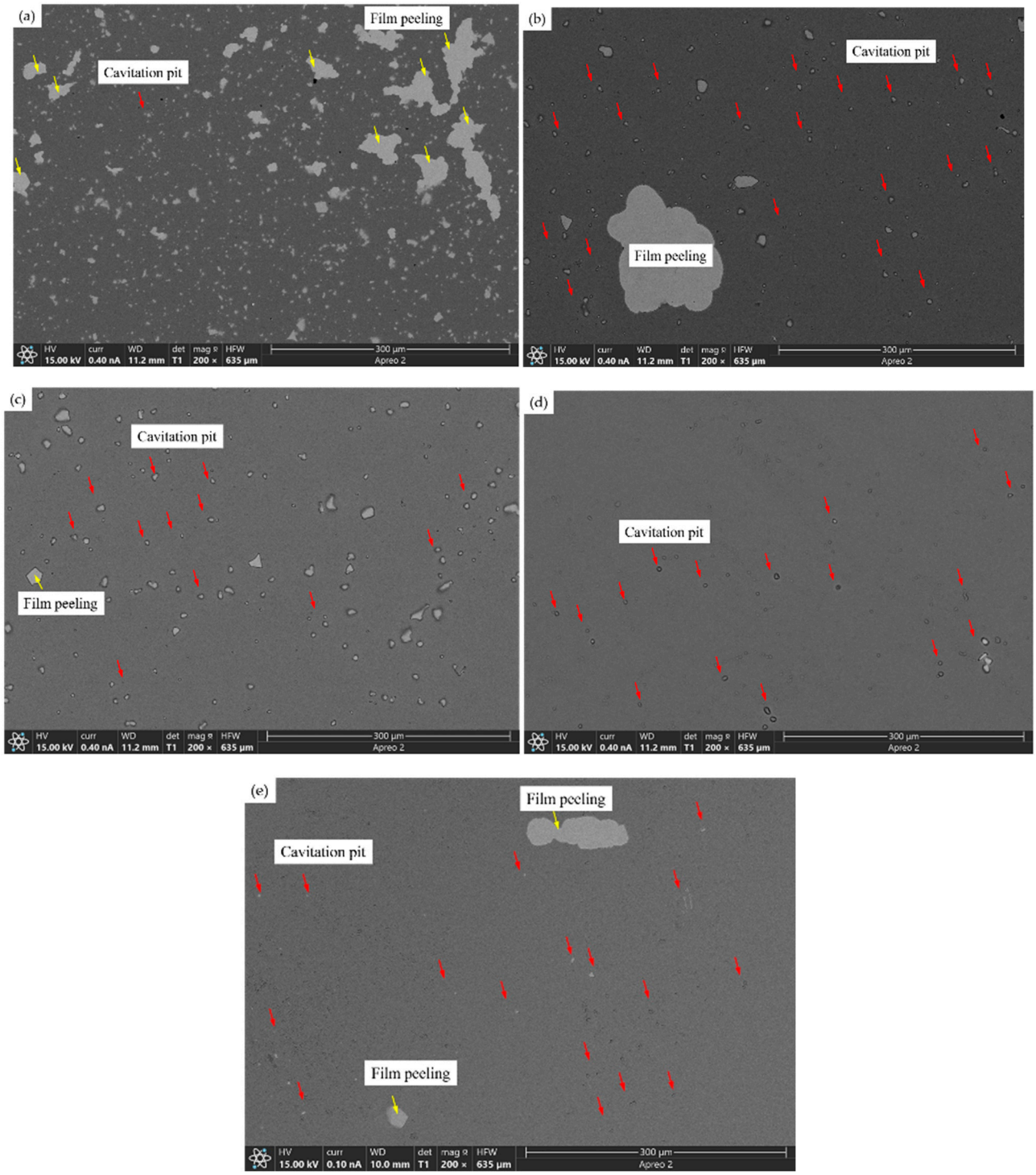

Figure 8. Surface morphologies of TiSiN/NiTiAlCoCrN nanomultilayer films with different modulation periods after 12 h of cavitation erosion (Red arrows indicate cavitation pits and yellow arrows indicate film peeling): (**a**) 5 nm; (**b**) 7 nm; (**c**) 9 nm; (**d**)11 nm; (**e**) 13 nm.

Figure 9 shows the element distributions of the cavitation pit of the TiSiN/NiTiAlCoCrN nanomultilayer film with 11 nm of modulation period. The Fe element appears, and Ni, Ti, Al, Co, and N elements disappear at the bottom of the cavitation pit, so the film breaks down. The O element appears in the wall of the cavitation pits, which means the oxidation reaction occurs during the cavitation process. Ni, Ti, Al, Co, and Cr elements react with oxygen to produce TiO_2, Al_2O_3, CoO, Cr_2O_3, etc. Cr_2O_3 and Al_2O_3 have a dense structure and higher hardness, which can better resist cavitation erosion during the experimental process. As the cavitation time increases, CoO reacts with oxygen to produce Co_3O_4, which also improves the cavitation erosion resistance.

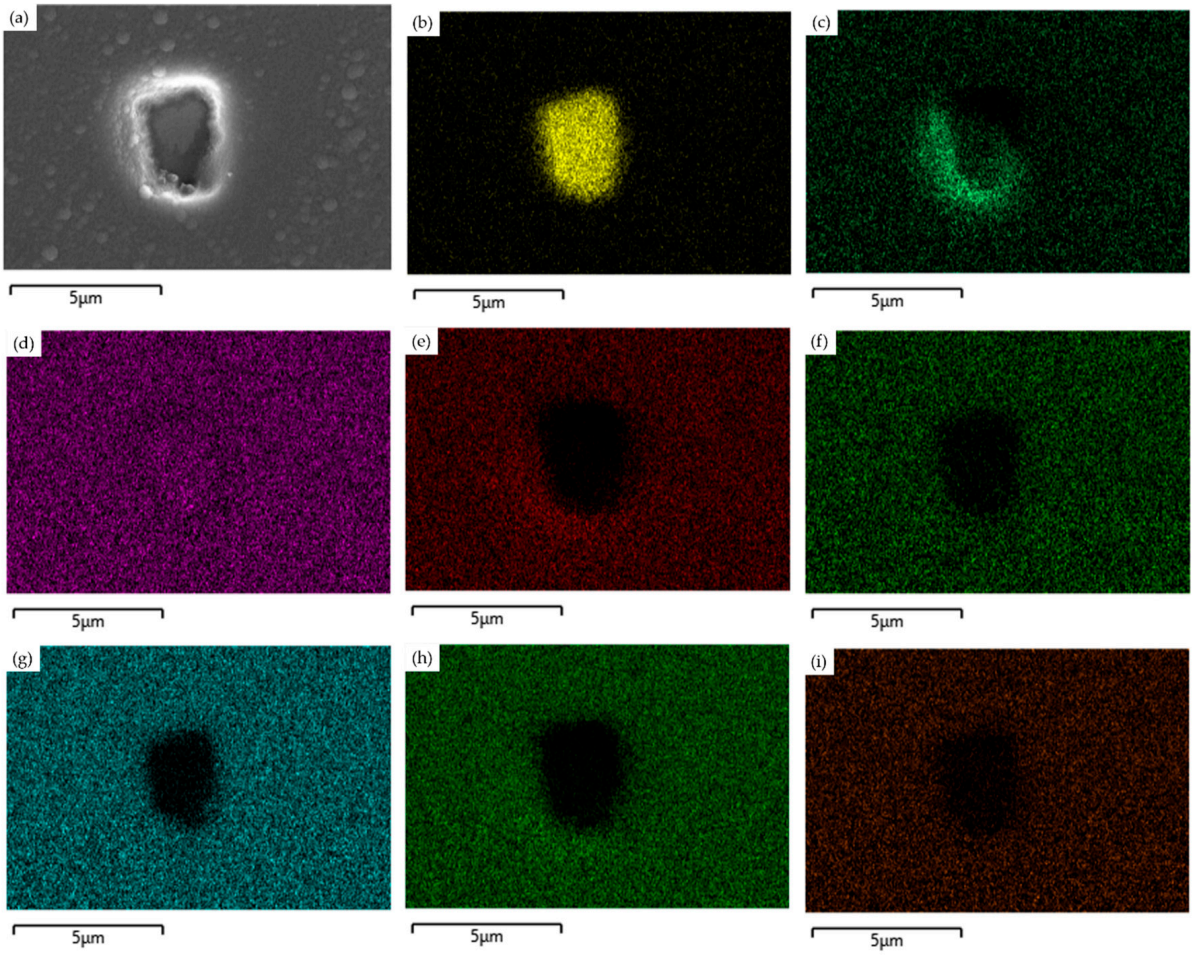

Figure 9. Element distribution of cavitation pits in TiSiN/NiTiAlCrCoN multilayer coatings with modulation period of 11 nm: (**a**) surface of cavitation pit; (**b**) Fe; (**c**) O; (**d**) Cr; (**e**) N; (**f**) Ni; (**g**) Ti; (**h**) Al; (**i**) Co.

4. Conclusions

TiSiN/NiTiAlCoCrN nanomultilayer films with different modulation periods were deposited on 304 stainless steel using a magnetron sputtering system. The metal elements were distributed evenly on the surface of the films. The N element content was from 40.52 at.% to 45.6 at.% in the films.

The TiSiN/NiTiAlCoCrN nanomultilayer films exhibit preferred orientation on the (200) plane. The plane spacing firstly decreases and then increases with increasing modulation periods. The alternating stress field is formed during the deposition process, which strengthens the film properties.

As the modulation period increases, the hardness, elastic modulus, and adhesive force firstly increase and then decrease. Firstly, the alternating stress field strengthens

the properties. Secondly, the interface between the TiSiN layer and NiTiAlCoCrN layer prevents dislocation expansion, which also improves the properties of the films.

As the modulation period increases, the cavitation erosion resistance firstly increases and then decreases. When the modulation period is 11 nm, the mass loss is the minimum, the number of cavitation pits is the least, and no film peeling occurs. The reason for this is that the nanomultilayer film with 11 nm modulation period has highest hardness and adhesive force, and the interfaces in the nanomultilayer film prevent the initiation and expansion of the cavitation pits. The oxidation generated during the cavitation process also improves the cavitation erosion resistance.

The TiSiN/NiTiAlCoCrN nanomultilayer film with a 11 nm modulation period exhibit the best properties. The film can be used as the coating of blades of turbines and water pumps, which can improve the corrosion erosion and prolong the life of blades.

Author Contributions: H.Y., L.S. and F.L. proposed the idea. H.Y., Y.Y. and H.L. carried out the experiments. H.Y., Z.D. and Y.Y. analyzed the experimental results. H.Y. and L.S. wrote the main manuscript text. All authors have read and agreed to the published version of the manuscript.

Funding: This research was funded by Natural Science Foundation of Beijing (Grant No. 3212003), and Yuyou Team of North China University of Technology (Grant No. 22XN746).

Institutional Review Board Statement: Not applicable.

Informed Consent Statement: Not applicable.

Data Availability Statement: All data are included in this published article.

Conflicts of Interest: The authors declare no conflict of interest.

References

1. Yin, D.; Liang, G.; Fan, S.; Li, S. Ultrasonic Cavitation Erosion Behavior of AlCoCr$_x$CuFe High Entropy Alloy Coatings Synthesized by Laser Cladding. *Materials* **2020**, *13*, 4067. [CrossRef] [PubMed]
2. Liu, Y.; Xiang, D.; Wang, K.; Yu, T. Corrosion of Laser Cladding High-Entropy Alloy Coatings: A Review. *Coatings* **2022**, *12*, 1669. [CrossRef]
3. Singh, R.; Tiwari, S.K.; Mishra, S.K. Cavitation Erosion in Hydraulic Turbine Components and Mitigation by Coatings: Current Status and Future Needs. *J. Mater. Eng. Perform.* **2011**, *21*, 1539–1551. [CrossRef]
4. Wei, X.; Zhu, W.; Ban, A.; Zhu, D.; Zhang, C.; Dong, H. Effects of Co addition on microstructure and cavitation erosion resistance of plasma sprayed TiNi based coating. *Surf. Coat. Technol.* **2021**, *409*, 126838. [CrossRef]
5. Ma, D.; Harvey, T.; Wellman, R.; Ehiasarian, A.; Hovsepian, P.E.; Sugumaran, A.; Purandare, Y.; Wood, R. Cavitation erosion performance of CrAlYN/CrN nanoscale multilayer coatings deposited on Ti6Al4V by HIPIMS. *J. Alloys Compd.* **2019**, *788*, 719–728. [CrossRef]
6. Szkodo, M.; Stanisławska, A.; Komarov, A.; Bolewski, Ł. Effect of MAO coatings on cavitation erosion and tribological properties of 5056 and 7075 aluminum alloys. *Wear* **2021**, *474–475*, 203709. [CrossRef]
7. Lin, J.; Hong, S.; Zheng, Y.; Sun, W.; Kang, M.; Fu, X. Cavitation erosion resistance in NaCl medium of HVOF sprayed WC-based cermet coatings at various flow velocities: A comparative study on the effect of Ni and CoCr binder phases. *Int. J. Refract. Met. Hard Mater.* **2021**, *94*, 105407. [CrossRef]
8. Fan, Q.; Chen, C.; Fan, C.; Liu, Z.; Cai, X.; Lin, S.; Yang, C. Ultrasonic induces grain refinement in gas tungsten arc cladding AlCoCrFeNi high-entropy alloy coatings. *Mater. Sci. Eng. A* **2021**, *821*, 141607. [CrossRef]
9. Zhu, Z.-X.; Liu, X.-B.; Liu, Y.-F.; Zhang, S.-Y.; Meng, Y.; Zhou, H.-B. Effects of Cu/Si on the microstructure and tribological properties of FeCoCrNi high entropy alloy coating by laser cladding. *Wear* **2023**, *512–513*, 204533. [CrossRef]
10. Ma, G.L.; Zhao, Y.; Cui, H.Z.; Song, X.J.; Wang, M.L.; Lee, K.M.; Gao, X.H.; Song, Q.; Wang, C.M. Addition Al and/or Ti induced modifications of microstructures, mechanical properties, and corrosion properties in CoCrFeNi high-entropy alloy coatings. *Acta Metall. Sin.* **2021**, *34*, 1087–1102. [CrossRef]
11. Qiu, X.W. Microstructure and corrosion properties of $Al_2CrFeCo_xCuNiTi$ high entropy alloys prepared by additive manufacturing. *J. Alloys Compd.* **2021**, *887*, 161422. [CrossRef]
12. Liang, H.; Hou, J.X.; Cao, Z.Q.; Jiang, L. Interesting 'island-like' microstructure and tribological evaluation of $Al_{1.5}CrFeNiWTi_{0.5}$ high entropy alloy coating manufactured by laser cladding. *Tribol. Int.* **2023**, *179*, 108171. [CrossRef]

13. Xiao, J.K.; Li, T.T.; Wu, Y.Q.; Chen, J.; Zhang, C. Microstructure and tribological properties of plasma-sprayed CoCrFeNi-based high-entropy alloy coatings under dry and oil-lubricated sliding conditions. *J. Therm. Spray Technol.* **2021**, *30*, 926–936. [CrossRef]
14. Huang, Y.; Hu, Y.; Zhang, M.; Mao, C.; Tong, Y.; Zhang, J.; Li, K.; Wang, K. On the enhanced wear resistance of laser-clad CoCrCuFeNiTix high-entropy alloy coatings at elevated temperature. *Tribol. Int.* **2022**, *174*, 107767. [CrossRef]
15. Lin, D.-Y.; Zhang, N.-N.; He, B.; Jin, B.-Q.; Zhang, Y.; Li, D.-Y.; Dong, F.-Y. Influence of laser re-melting and vacuum heat treatment on plasma-sprayed FeCoCrNiAl alloy coatings. *J. Iron Steel Res. Int.* **2017**, *24*, 1199–1205. [CrossRef]
16. Doan, D.-Q.; Nguyen, V.-H.; Tran, T.-V.; Hoang, M.-T. Atomic-scale analysis of mechanical and wear characteristics of AlCoCrFeNi high entropy alloy coating on Ni substrate. *J. Manuf. Process* **2023**, *85*, 1010–1023. [CrossRef]
17. Wei, Z.; Wu, Y.; Hong, S.; Cheng, J.; Qiao, L.; Cheng, J.; Zhu, S. Ultrasonic cavitation erosion behaviors of high-velocity oxygen-fuel (HVOF) sprayed AlCoCrFeNi high-entropy alloy coating in different solutions. *Surf. Coat. Technol.* **2021**, *409*, 126899. [CrossRef]
18. Xu, J.; Peng, S.; Li, Z.; Jiang, S.; Xie, Z.-H.; Munroe, P.; Lu, H. Remarkable cavitation erosion–corrosion resistance of CoCrFeNiTiMo high-entropy alloy coatings. *Corros. Sci.* **2021**, *190*, 109663. [CrossRef]
19. Straumal, B.; Rabkin, E.; Lopez, G.A.; Korneva, A.; Kuzmin, A.; Gornakova, A.; Straumal, A.; Baretzky, B. Grain Boundary Wetting Phenomena in High Entropy Alloys Containing Nitrides, Carbides, Borides, Silicides, and Hydrogen: A Review. *Crystals* **2021**, *11*, 1540.
20. Wu, T.; Chen, Y.; Lin, B.; Yu, L.; Gui, W.; Li, J.; Wu, Y.; Zeng, D. Effects of WC on the Microstructure, Wear and Corrosion Resistance of Laser-Deposited CoCrFeNi High Entropy Alloy Coatings. *Coatings* **2022**, *12*, 985. [CrossRef]
21. Wei, Z.; Wu, Y.; Hong, S.; Cheng, J.; Qiao, L.; Cheng, J.; Zhu, S. Effect of WC-10Co on cavitation erosion behaviors of AlCoCrFeNi coatings prepared by HVOF spraying. *Ceram. Int.* **2021**, *47*, 15121–15128. [CrossRef]
22. Bao, Y.; Guo, L.; Zhong, C.; Song, Q.; Yang, K.; Jiang, Y.; Wang, Z. Effects of WC on the cavitation erosion resistance of $FeCoCrNiB_{0.2}$ high entropy alloy coating prepared by laser cladding. *Mater. Today Commun.* **2021**, *26*, 102154. [CrossRef]
23. Lan, L.; Wang, X.; Guo, R.; Yang, H.; Qiao, J. Effect of environments and normal loads on tribological properties of nitrided $Ni_{45}(FeCoCr)_{40}(AlTi)_{15}$ high-entropy alloys. *J. Mater. Sci. Technol.* **2019**, *42*, 85–96. [CrossRef]
24. Xu, Y.; Li, G.; Xia, Y. Synthesis and characterization of super-hard AlCrTiVZr high-entropy alloy nitride films deposited by HiPIMS. *Appl. Surf. Sci.* **2020**, *523*, 146529. [CrossRef]
25. Chen, L.Q.; Li, W.; Liu, P.; Zhang, K.; Ma, F.C.; Chen, X.H.; Zhou, H.L.; Liu, X.K. Microstructure and mechanical properties of (AlCrTiZrV)Nx high-entropyalloy nitride films by reactive magnetron sputtering. *Vacuum* **2020**, *181*, 109706. [CrossRef]
26. Chen, W.; Yan, A.; Wang, C.; Deng, Y.; Chen, D.; Xiao, H.; Zhang, D.; Meng, X. Microstructures and mechanical properties of AlCrN/TiSiN nanomultilayer coatings consisting of fcc single-phase solid solution. *Appl. Surf. Sci.* **2020**, *509*, 145303. [CrossRef]
27. Chang, Y.-Y.; Yang, Y.-J.; Weng, S.-Y. Effect of interlayer design on the mechanical properties of AlTiCrN and multilayered AlTiCrN/TiSiN hard coatings. *Surf. Coat. Technol.* **2020**, *389*, 125637. [CrossRef]
28. Krella, A.K.; Czyzniewski, A.; Gilewicz, A.; Gajowiec, G. Experimental Study of the Influence of Deposition of Multilayer CrN/CrCN PVD Coating on Austenitic Steel on Resistance to Cavitation Erosion. *Coatings* **2020**, *10*, 487. [CrossRef]
29. Li, B.H.; Ma, X.; Li, W.; Zhai, Q.; Liu, P.; Zhang, K.; Ma, F.; Wang, J. Effect of SiC thickness on microstructure and mechanical properties of (AlCrTiZrV)N/SiC nano-multilayers film synthesized by reactive magnetron sputtering. *Thin Solid Film.* **2021**, *730*, 138724. [CrossRef]
30. Bagdasaryan, A.A.; Pshyk, A.V.; Coy, L.E.; Kempinski, M.; Pogrebnjak, A.D.; Beresnev, V.M.; Jurga, S. Structural and mechanical characterization of (TiZrNbHfTa)N/WN multilayered nitride coatings. *Mater. Lett.* **2018**, *229*, 364–367. [CrossRef]
31. Lu, Z.; Mao, Y.; Ren, S.; Pu, J.; Fu, Z.; Fan, X.; Gao, S.; Fan, J. A novel design of VAlTiCrCu/WC alternate multilayer structure to enhance the mechanical and tribo-corrosion properties of the high-entropy alloy coating. *Mater. Charact.* **2021**, *176*, 111115. [CrossRef]
32. He, H.J.; Liu, C.H.; He, L.X.; Wang, G.C.; Zhang, W.; Zhao, S.; Xiang, Y.; Yi, J. Microstructure, mechanical properties and high temperature corrosion of $[AlTiCrNiTa/(AlTiCrNiTa)N]_{20}$ high entropy alloy multilayer coatings for nuclear fuel cladding. *Vacuum* **2023**, *212*, 112057. [CrossRef]
33. Yan, H.J.; Liu, Y.F.; Mi, Z.F.; Si, L.N.; Dou, Z.L.; Liu, F.B. Effect of nitrogen-argon flow ratio on cavitation resistance of NiTiAlCrN coating. *J. Funct. Mater.* **2023**, *54*, 01007–01011.
34. Sui, X.; Li, G.; Jiang, C.; Wang, K.; Zhang, Y.; Hao, J.; Wang, Q. Improved toughness of layered architecture TiAlN/CrN coatings for titanium high speed cutting. *Ceram. Int.* **2018**, *44*, 5629–5635. [CrossRef]
35. Wei, Y.Q.; Zong, X.Y.; Jiang, Z.Q. Characterization and mechanical properties of TiN/TiAlN multilayer coatings with different modulation periods. *Int. J. Adv. Manuf. Technol.* **2018**, *96*, 1677–1683.
36. Zhai, Q.Q.; Li, W.; Liu, P. Mechanical Behavior and Thermal Stability of (AlCrTiZrMo)N/ZrO_2 Nano-Multilayered High-Entropy Alloy Film Prepared by Magnetron Sputtering. *Crystals* **2022**, *12*, 232. [CrossRef]
37. Chen, W.J.; Wang, J.j.; Liu, P. Effects of Y addition on the microstructures and mechanical behavior of ZrOxNy/V_2O_3-Y nano-multilayered films. *Mater. Sci. Eng. A* **2023**, *864*, 144555. [CrossRef]
38. Koehler, J.S. Attempt to Design a Strong Solid. *Phys. Rev. B* **1970**, *2*, 547–551. [CrossRef]
39. Xu, Y.X.; Chen, L.; Pei, F.; Du, Y. Structure and thermal properties of TiAlN/CrN multilayered coatings with various modulation ratios. *Surf. Coat. Technol.* **2016**, *304*, 512–518. [CrossRef]

40. Chang, Y.-Y.; Chang, H.; Jhao, L.-J.; Chuang, C.-C. Tribological and mechanical properties of multilayered TiVN/TiSiN coatings synthesized by cathodic arc evaporation. *Surf. Coat. Technol.* **2018**, *350*, 1071–1079. [CrossRef]
41. Yu, P.; Li, W.; Liu, P.; Zhang, K.; Ma, F.; Chen, X.; Feng, R.; Liaw, P.K. Microstructural and electrical behavior of NiCr/Al nanomultilayered films prepared by magnetron sputtering. *J. Alloys Compd.* **2022**, *911*, 165012. [CrossRef]